Inorganica Chimica Acta 514 (2021) 120003

Contents lists available at ScienceDirect

Inorganica Chimica Acta

journal homepage: www.elsevier.com/locate/ica

Research paper

Azido- and amino-substituted dipicolinates for the sensitization of the luminescent lanthanides Eu^{III} and Tb^{III}

Katherine R. Johnson, Ana de Bettencourt-Dias*

Department of Chemistry, University of Nevada, Reno, 1664 N. Virginia Street, Reno, NV 89557, United States

ARTICLE INFO

Keywords:
Lanthanide complexes
Amido-substituted dipicolinato
Azido-substituted dipicolinato
Luminescence
X-ray crystallography

ABSTRACT

Dipicolinate-based ligands substituted with azido- or amino- functional groups were synthesized and characterized. Crystal structures of $\mathbf{E_{N3}}$, $\mathbf{C_{N3}}$, $\mathbf{C_{NH2}}$, and $\mathbf{E_{NH2}}$ were obtained, and the ability of these compounds to sensitize Ln^{III} luminescence (Ln^{III} = Eu^{III} and Tb^{III}) was explored. Luminescence efficiencies of Eu^{III} and Tb^{III} were determined and are ϕ_{Eu} = 0.11%, 0.15%, and 13.8% for $[Ln(\mathbf{C_{N3}})_3]^{3+}$, $[Ln(\mathbf{E_{N3}})_3]^{3+}$, $[Ln(\mathbf{C_{NH2}})_3]^{3+}$, respectively, and ϕ^{Tb} = 0.30%, 0.27%, and 28.9% for $[Ln(\mathbf{C_{N3}})_3]^{3+}$, $[Ln(\mathbf{E_{N3}})_3]^{3+}$, $[Ln(\mathbf{E_{NH2}})_3]^{3+}$. The highest luminescence efficiencies are ϕ_{Eu} = 14.4% for $[Eu(\mathbf{E_{NH2}})_3]^{3+}$ and ϕ_{Tb} = 29.7% for $[Tb(\mathbf{C_{NH2}})_3]^{3+}$. Similar ^{1}S and ^{3}T excited state energies were observed for all ligands and did not explain the observed discrepancies in luminescence efficiency of their Tb^{III} and Eu^{III} complexes. Further analysis revealed that the azido-derivatives were not photostable, which likely contributed to the low luminescence efficiency.

1. Introduction

The luminescence properties of lanthanide (Ln^{III}) complexes are attractive for use as sensors [1–4], light-emitting diodes [5,6], and in immunoassays[7] due to their large Stokes shifts of sensitized emission, color purity, and long-lived excited states. A few examples of luminescent Ln^{III} complexes (Fig. 1) include highly luminescent visible emitting Eu^{III} and Tb^{III} complexes (**1**), [8] water-soluble visible and NIR emitting Ln^{III} complexes (**2**), [9] a 2,2‘,2‘ ‘,2‘ “- [4‘-(aminobiphenyl-4-yl)-2,2‘:6‘,2‘ ‘-terpyridine- 6,6‘ ‘-diyl]bis(methylenenitrilo)]tetrakis (acetato) (ATBTA) Eu^{III} complex appended to agarose beads for Eu^{III} luminescence imaging of zebrafish embryos (**3**), [10] a turn-on Tb^{III} complex for the detection of nitroreductases in living bacteria (**4**), [11] and pyclen-based Ln^{III} luminescent complexes as *in vitro* and *in vivo* bioprobes using one- and two-photon excitation (**5**).[12]

As shown in Fig. 2, Ln^{III} sensitization begins with the population of the ligand excited singlet state (^{1}S) after photon absorption (hν). Subsequent intersystem crossing (ISC) generates a long-lived excited triplet state (^{3}T). If the energy of ^{3}T is well matched to the emissive excited state of the Ln^{III} (*f**),[13] energy transfer (ET) can occur, and the Ln^{III} decays by luminescence (L) to the ground state. Nonradiative (NR) pathways can lead to quenching of excited states. Other possible radiative processes are fluorescence (F) and phosphorescence (P).

The overall efficiency of sensitized Ln^{III} emission (ϕ_{Ln}) is described by equation (1), which is a product of the efficiencies of the consecutive individual energy transfer steps. ϕ_{ISC} is the efficiency of intersystem crossing, and ϕ_{ET} is the efficiency of the energy transfer from ^{3}T to *f**. The combined efficiency of these two steps corresponds to the sensitization efficiency (η_{sens}) of the ligand. The efficiency of the last step, L, is the intrinsic quantum yield of luminescence of the metal ion (ϕ_{Ln}^{Ln}).

$$\phi_{Ln} = \phi_{ISC} \times \phi_{ET} \times \phi_{Ln}^{Ln} = \eta_{sens} \times \phi_{Ln}^{Ln} \quad (1)$$

The dipicolinate scaffold has been widely used in our group [9,14–16] and by others[17–27] to study the luminescence properties of Ln^{III} complexes because of the ability to easily functionalize the pyridine at the *para*-position. We reported $^1O_2$ generating Ln^{III} luminescent complexes that featured 1,8-naphthalimide or oligothiophene moieties at the para position of dipicolinato chelators.[14,15] Our group also reported compounds that display Eu^{III} and Yb^{III} emission upon one- and two-photon excitation using a dipicolinate derivative. [28]

Here, we describe four chelators featuring terminal azido- or amino-groups, all of which were previously isolated as intermediates.[15,29] Compounds that feature terminal azides or amines, like the compounds studied here, have significant utility in organic syntheses such as azide/alkyne click chemistry, Schiff base formation, and are important for small molecule synthesis.[30,31] Furthermore, they are important in systems that are biologically relevant,[29,32–34] and thus, their luminescent Ln^{III} complexes might be useful in bioimaging or other medicinal applications.[2,10,12,29,32,35–37] These compounds and

* Corresponding author.
E-mail address: abd@unr.edu (A. de Bettencourt-Dias).

https://doi.org/10.1016/j.ica.2020.120003
Received 30 June 2020; Received in revised form 1 September 2020; Accepted 2 September 2020
Available online 05 September 2020

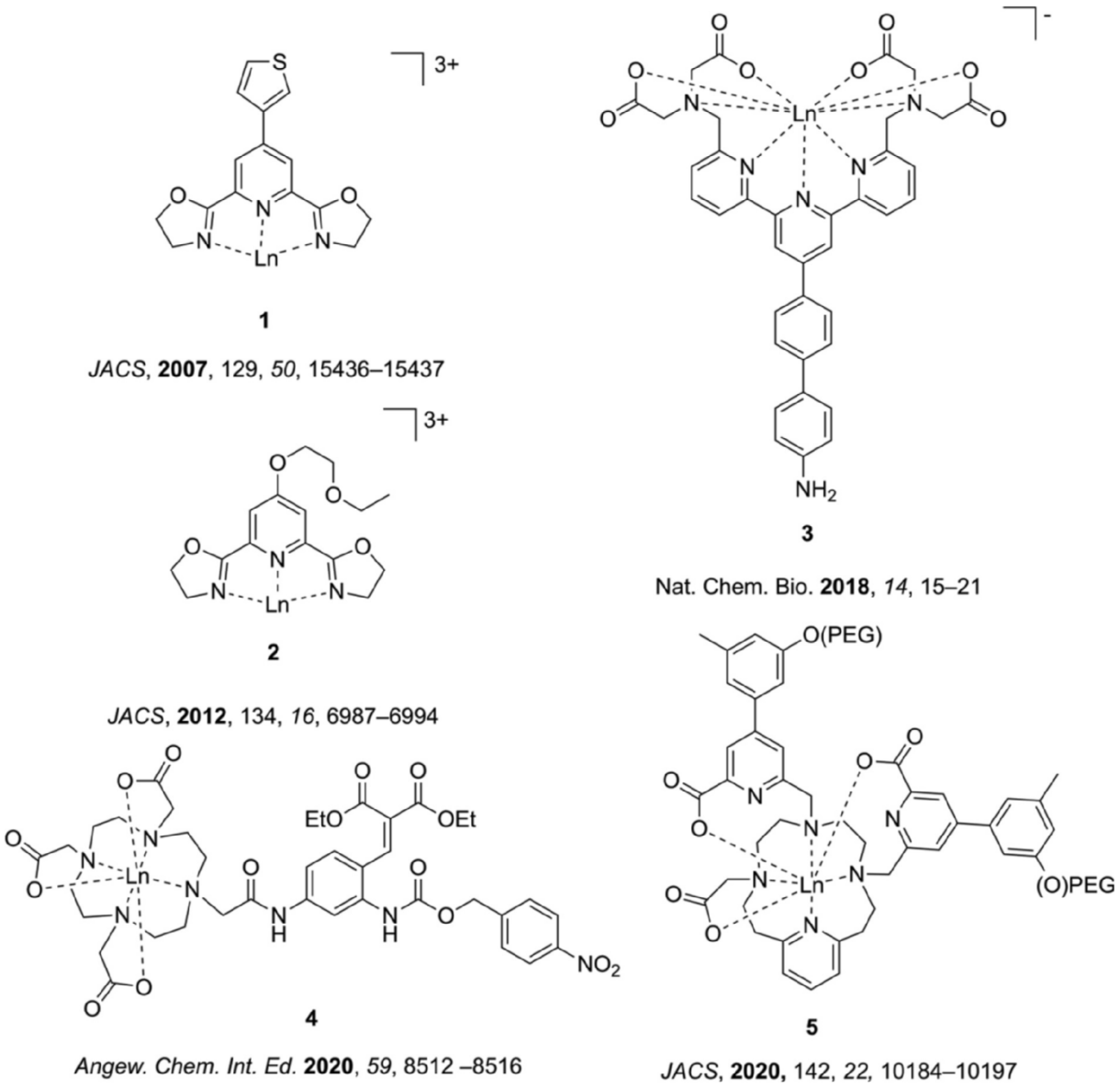

Fig. 1. Examples of luminescent Ln^{III} complexes.

their Eu^{III} and Tb^{III} complexes were synthesized, and their photophysical properties were explored.

2. Experimental section

2.1. Materials and methods

All commercially obtained reagents were of analytical grade and were used as received. Solvents were dried and purified by standard methods unless otherwise noted. All synthetic steps were completed under N_2 unless otherwise specified.

All data presented in this work are the average of at least three independent measurements.

Nuclear Magnetic Resonance (NMR) spectroscopy. NMR spectra were recorded on Varian 400 or 500 MHz spectrometers at 25.0 ± 0.1 °C with chemical shifts reported (δ, ppm) against tetramethylsilane (TMS, 0.00 ppm).

X-ray crystallography. Crystal data, data collection, and refinement details for $\mathbf{C_{N3}}$, $\mathbf{C_{NH2}}$, $\mathbf{E_{N3}}$, and $\mathbf{E_{NH2}}$ are given below. Suitable crystals were mounted on a glass fiber and placed in a low-temperature nitrogen stream of a Bruker SMART CCD area detector diffractometer. A full sphere of data was collected using a graphite-monochromated Mo-Kα radiation source (λ = 0.71073 Å). Multi-scan absorption corrections were applied using SADABS.[38] The structures were solved by direct methods and refined by least-square methods on F^2 using the SHELXTL [39] programming package. All non-hydrogen atoms were refined anisotropically. The hydrogen atoms were added geometrically, and their parameters were constrained to the parent site.

CCDC 1995777 ($\mathbf{C_{N3}}$), 1995778 ($\mathbf{E_{N3}}$), 1995779 ($\mathbf{E_{NH2}}$), and 1995780 ($\mathbf{C_{NH2}}$) contain the supplementary crystallographic data of the molecular structures obtained for this paper and can be obtained free of charge via www.ccdc.cam.ac.uk/conts/retrieving.html or from the Cambridge Crystallographic Data Centre, 12 Union Rd. Cambridge CB2 1EZ, UK; fax: +44–1223-336033; or deposit@ccdc.cam.ac.uk.

Absorption spectroscopy. Absorption spectra were measured on a Perkin Elmer Lambda 35 spectrometer equipped with deuterium and tungsten halogen lamps (Perkin Elmer) and a concave grating with 1053 lines/mm. They were collected using a scan speed of 480 nm/min in the range of 225–600 nm with a photodiode detector. All spectra were background corrected, using solvent as the blank. Spectra of the ligands and their complexes were collected at 25.0 ± 0.1 °C. The temperature of the cell holder was controlled with a circulating bath.

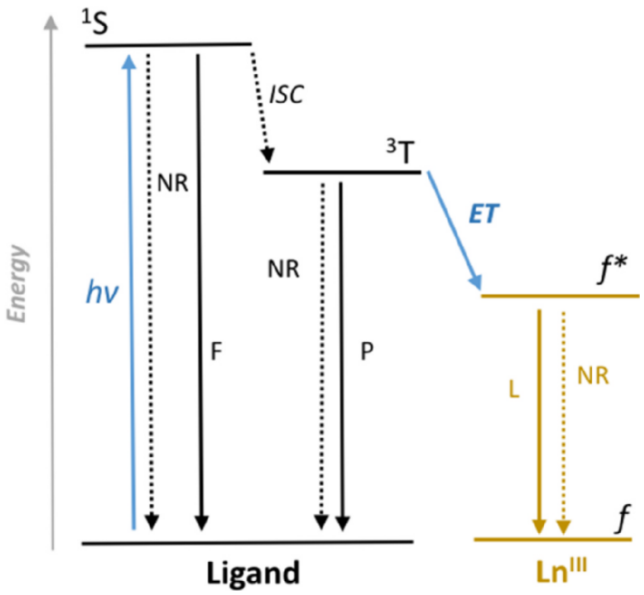

Fig. 2. Energy level diagram illustrating the mechanism for Ln^{III} sensitization. Energy hυ is absorbed by the ligand to populate a singlet excited state (^{1}S). A triplet excited state (^{3}T) is populated after intersystem crossing (ISC). ^{3}T can transfer energy (ET) to the emissive *f** excited state, which decays by luminescence (L) to the ground state. Nonradiative (NR) pathways can lead to quenching of excited states. Other possible radiative processes are fluorescence (F) and phosphorescence (P). Energy levels are not drawn to scale.

Excitation and emission spectroscopy. Emission and excitation spectra of the ligands and their Ln^{III} complexes were obtained at 25.0 ± 0.1 °C (the temperature of the cell holder was controlled with a circulating bath) in a Fluorolog-3 fluorimeter (Horiba FL3-22-iHR550), with a 1200 grooves/mm excitation monochromator with gratings blazed at 330 nm and a 1200 grooves/mm or 600 grooves/mm emission monochromator with gratings blazed at 500 nm or 1000 nm for the UV–Vis or NIR range, respectively. A 450W ozone-free xenon lamp (Ushio) was used as the radiation source. The emission spectra were measured in the range 350–800 nm using a Hamamatsu 928P detector and in the range 800–1600 nm using a Hamamatsu 5509–73 detector cooled with liquid N_2. All excitation and emission spectra were corrected for instrumental function.

Emission titrations with Tb^{III} nitrate. A solution of the ligand (5×10^{-5} M) was titrated with aliquots of $Tb(NO_3)_3$ (1.0–1.3 mM), and the resulting emission spectra were measured (Fig. 6, 20–22). The maximum intensity of the $^5D_4 \rightarrow {}^7F_5$ was plotted as a function of Tb^{III}:ligand ratio.

Excited state determination. The ^{1}S and ^{3}T energies were obtained at ~77 K by deconvoluting the fluorescence and phosphorescence spectra of the gadolinium complexes into their Franck-Condon progression and are reported as the 0–0 transition [40].

Emission efficiency measurements. The efficiency of sensitized emission ϕ_{Ln}, the fluorescence efficiency ϕ^F, and efficiency of $^1O_2$ generation ϕ_{1O2} were determined by the dilution method using Equation (2).[41]

$$\phi_x = \frac{Grad_x}{Grad_{std}} \times \frac{n_x^2}{n_{std}^2} \times \frac{I_{std}}{I_x}\phi_{std} \quad (2)$$

Grad is the slope of the plot of the emission area as a function of the absorbance, *n* is the refractive index of the solvent, *I* is the intensity of the excitation source at the excitation wavelength used and ϕ is the quantum yield for sample, *x,* and standard, *std.*

Standards for emission quantum yield measurements were Cs_3[Eu(dpa)$_3$] (ϕ_{Eu} = 24%, 7.5 × 10^{-5} M in aqueous TRIS/HCl buffer (0.1 M, pH ~ 7.4)), for Eu^{III} luminescence and Cs_3[Tb(dpa)$_3$] (ϕ^{Tb} = 22%, 9 × 10^{-5} M in aqueous TRIS/HCl buffer (0.1 M, pH ~ 7.4)) for Tb^{III} luminescence.[18,19] The excitation wavelength for both sample and standard were chosen to ensure a linear relationship between the intensity of emitted light and the concentration of the absorbing/emitting species ($A \leq 0.05$).

The intrinsic quantum yield for Eu^{III} complexes ϕ_{Eu}^{Eu} was determined using equation (2).

$$\phi_{Eu}^{Eu} = \frac{A_{rad}}{A_{tot}} \quad (3)$$

A_{tot} is the total emission rate ($A_{tot} = k_R + k_{NR} = 1/\tau_{exp}$), k_R is the radiative rate constant, k_{NR} is the non-radiative decay constant, τ_{exp} is the observed excited state lifetime. For Eu^{III}, A_{rad}, the radiative emission rate, can be determined using equation (4).[42]

$$A_{rad} = A_{MD,0} \times n^3\left(\frac{I_{tot}}{I_{MD}}\right) \quad (4)$$

I_{tot} and I_{MD} are the total integrated emission spectrum and the area of the $^5D_0 \rightarrow {}^7F_1$ transition of Eu^{III}, respectively, and $A_{MD,0}$ is Einstein coefficient of spontaneous emission ($A_{MD,0}$ = 14.65 s^{-1}).[43]

The sensitization efficiency (η_{sens}) was determined using equation (1).[22]

Infrared Spectroscopy. All FT-IR spectra were measured on a Nicolet 6700 FT-IR in ATIR mode. The IR data for each sample were collected in the range 4000–590 cm^{-1}, with 100 scans at 1 cm^{-1} resolution per spectrum. A background correction for CO_2 and H_2O was done.

Mass Spectrometry. Electrospray ionization mass spectra (ESI-MS) were collected in positive ion mode on an Agilent model G6230A with a QTOF analyzer in the high-resolution mode for the ligands and the metal complexes. The samples were prepared by diluting acetonitrile solutions to a concentration of ~0.5 mg/mL and passing through a 0.2 mm microfilter.

2.2. Synthesis of C_{N3}, C_{NH2}, E_{N3}, and E_{NH2}

4-Chloropyridine-2,6-dicarboxamide. Thionyl chloride (10 mL) and anhydrous DMF (0.25 mL) were added to chelidamic acid (3.10 g) and refluxed overnight (16 h). The resulting yellow solution was cooled to 45 °C, and the excess solvent was decanted, yielding a light-yellow precipitate. The reaction was cooled to 0 °C, and diethylamine (15.5 mL) was added dropwise over 30 min. The reaction was warmed to room temperature and stirred for 1 h, then heated to 40 °C for 3 h before quenching with water (7 mL). The desired product was extracted with $CHCl_3$ (3 × 20 mL). The combined organic phases were washed with water (3 × 50 mL) and brine (3 × 50 mL), dried over Na_2SO_4, and filtered. Excess solvent was removed under reduced pressure, and the product, a beige powder, was recrystallized from hexanes. Yield: 3.79 g, *79%*. ^{1}H NMR (400 MHz, DMSO-d_6) δ (ppm): 7.62 (s, 2H, *pyr.*), 3.55 (q, 4H, *J* = 7.0 Hz, *CH_2*), 3.33 (q, 4H, *J* = 7.0 Hz, *CH_2*), 1.25 (t, 6H, *J* = 7.2 Hz, *CH_3*), 1.15 (t, 6H, *J* = 7.2 Hz, *CH_3*).

4-Azidopyridine-2,6-dicarboxamide (***C_{N3}***). 4-Chloropyridine-2,6-dicarboxamide (860 g, 2.75 mmol) was dissolved in anhydrous DMF (10 mL). NaN_3 (1.79 g) was added, and the resulting suspension was heated to 70 °C for 24 h. The reaction was quenched with water (8 mL), and the solution was extracted with ethyl acetate (3 × 20 mL). The combined organic layers were washed with water (3 × 50 mL) and brine (3 × 50 mL), dried over Na_2SO_4, and filtered. Excess solvent was removed under reduced pressure to yield the product as a yellow powder. Yield: 559 mg, *64%*. ^{1}H NMR (400 MHz, DMSO-d_6) δ (ppm): 7.29 (s, 2H, *pyr.*), 3.44 (q, 4H, *J = 7.0 Hz, CH_2*), 3.19 (q, 4H, *J = 7.0 Hz, CH_2*), 1.14 (t, 6H, *J* = 7.2 Hz, *CH_3*), 1.05 (t, 6H, *J* = 7.2 Hz, *CH_3*). ^{13}C NMR (100 MHz, $CDCl_3$) δ (ppm): 167.28, 155.36, 144.06, 43.23, 40.24, 14.24, 12.72. FT- IR (neat, ν, cm^{-1}): 3070–2823, (ν_{max} = 2979, C—H and C—C), 2105 (- N_3), 1630 (as. *N*-C=O), 1589 (pyr. C=N). ESI-HRMS $C_{15}H_{22}KN_6O_2^+$: 357.1526 (exp.), 357.1436 (calc.).

4-Aminopyridine-2,6-dicarboxamide (***C_{NH2}***). 4-Azidopyridine-2,6-

dicarboxamide (210 mg) and Pd/C (117 mg, 10%) was added to anhydrous ethyl acetate (12 mL). H_2 was bubbled through the solution while stirring at room temperature for 16 h. The solution was filtered, and the excess solvent was removed under reduced pressure. The desired product was isolated as a white powder. Yield: 167 mg, *73%*. ^{1}H NMR (400 MHz, $CDCl_3$) δ (ppm): 6.79 (s, 2H, *pyr.*), 3.52 (q, 4H, J = 7.0 Hz, CH_2), 3.44 (q, 4H, J = 7.0 Hz CH_2), 1.22 (t, 6H, J = 7.2 Hz, CH_3), 1.12 (t, 6H, J = 7.2 Hz, CH_3). ^{13}C NMR (100 MHz, $CDCl_3$) δ (ppm): 168.64, 154.69, 154.16, 109.00, 43.15, 39.99, 14.26, 12.79. IR (neat, ν, cm^{-1}): 3510–3375 (ν_{max} = 3413, *br.* –NH_2), 3375–3160, (ν_{max} = 3329, CO-NEt_2), 3094–2800, (ν_{max} = 2983, C—H and C—C), 1632 (as. *N*-C═O), 1589 (pyr. C═N). ESI-HRMS $C_{15}H_{25}N_4O_2^+$: 293.4005 (exp.), 293.3905 (calc.).

4-Chloropyridine-2,6-diethylester. Thionyl chloride (10 mL) and anhydrous DMF (0.25 mL) were added to chelidamic acid (3.10 g), refluxed, and stirred overnight (16 h). The resulting yellow solution was cooled to 45 °C, and the excess solvent was decanted, yielding a light-yellow precipitate. This precipitate was cooled to 0 °C, and anhydrous ethanol (13 mL) was added dropwise over 30 min. The reaction was warmed to room temperature and stirred for one hour. Excess solvent was removed under reduced pressure, and a white powder was isolated. This powder was re-dissolved in chloroform, washed with cold water (3 × 30 mL), and brine (3 × 30 mL). The organic phase was dried over Na_2SO_4, filtered, and the excess solvent was removed under reduced pressure. The resulting yellow oil was recrystallized from ethanol at 0 °C, filtered, and the product was isolated as a beige powder. Yield: 2.88 g, *72%*. ^{1}H NMR (400 MHz, DMSO-d_6) δ (ppm): 8.26 (s, 2H, *pyr.*), 4.49 (q, 4H, J = 7.1 Hz, CH_2), 1.46 (t, 6H, J = 7.1 Hz, CH_3).

*4-Azidopyridine-2,6-diethylester (**E_{N3}**).* 4-Chloropyridine-2,6-diethyl ester (860 mg) was dissolved in anhydrous DMF (10 mL). NaN_3 (1.79 g) was added, and the resulting suspension was heated to 70 °C overnight. After 24 h, the reaction mixture was extracted with ethyl acetate (3 × 20 mL) and washed with water (3 × 50 mL) and brine (3 × 50 mL). The organic layer was recovered, and over Na_2SO_4 and filtered. Excess solvent was removed under reduced pressure, and the product was isolated as a white powder. Yield: 357 mg, *32%*. ^{1}H NMR (400 MHz, DMSO-d_6) δ (ppm): 7.84 (s, 2H, *pyr.*), 4.48 (q, 4H, J = 7.1 Hz, CH_2), 1.35 (t, 6H, J = 7.1 Hz, CH_3). ^{13}C NMR (100 MHz, DMSO-d_6) δ (ppm): 164.13, 151.61, 149.87, 118.49, 62.29, 14.55. IR (neat, ν, cm^{-1}): 3110–2830, (ν_{max} = 2987, C—H and C—C), 2130 (- N_3), 1720 (as. *N*-C═O), 1585 (pyr. C═N). ESI-HRMS $C_{11}H_{13}N_4O_4^+$: 265.0849 (exp.), 265.0931 (calc.).

*4-Aminopyridine-2,6-diethylester (**E_{NH2}**).* 4-Azidopyridine-2,6-diethylester (250 mg, 0.932 mmol) and Pd/C (55.2 mg, 10%) were added to anhydrous ethyl acetate (10 mL). H_2 was bubbled through the solution while stirring at room temperature for 16 h. The solution was filtered, and the excess solvent was removed under reduced pressure to yield the product as a white powder. Yield: 160 mg, *72%*. ^{1}H NMR (400 MHz, DMSO-d_6) δ (ppm): 7.33 (s, 2H, *pyr.*), 6.69 (s, 2H, NH_2), 4.29 (q, 4H, J = 7.1 Hz, CH_2), 1.30 (t, 6H, J = 7.1 Hz, CH_3). ^{13}C NMR (100 MHz, DMSO-d_6) δ (ppm): 165.41, 156.64, 148.82, 112.36, 61.49, 14.63. IR (neat, ν, cm^{-1}): 3490–3385 (ν_{max} = 3417, - NH_2), 3385–3130, (ν_{max} = 3335,CO-NEt_2), 3090–2790, (ν_{max} = 2921, C—H and C—C), 1721 (as. *N*-C═O), 1592 (pyr. C═N). ESI-HRMS $C_{11}H_{15}N_2O_4^+$: 239.1096 (exp.), 239.1026 (calc.).

2.3. Synthesis of Ln^{III} complexes

All metal complexes were prepared by mixing one equivalent of dry $Ln(NO_3)_3$ (Ln^{III} = Eu^{III}, Tb^{III}, or Gd^{III}) with 3 equivalents of either **C_{N3}**, **C_{NH2}**, **E_{N3}**, or **E_{NH2}** in acetonitrile (~10 mL) and refluxed for 16 h. After solvent evaporation, the salts $[Ln(\mathbf{L})_3](NO_3)_3$ (**L** = **C_{N3}**, **C_{NH2}**, **E_{N3}**, or **E_{NH2}**) were obtained as white powders in 92 – 97% yield and characterized using mass spectrometry (Figs. S24–S35) and FT-IR spectroscopy in selected cases (Fig. S36). FT-IR data indicates that the carbonyl stretches do not change appreciably between ligands and Ln^{III} complexes and were not further pursued. The resulting solids were dissolved in spectrophotometric grade acetonitrile for photophysical characterization. Attempts to isolate X-ray quality single crystals of these metal complexes are ongoing.

$[Gd(\mathbf{C_{N3}})_3]^{3+}$ + $2NO_3^-$
Yield: 92%
ESI-MS: $[C_{45}H_{66}GdN_{20}O_{12}]^+$, *m/z*: 1236.4390 (exp.), 1236.4405 (calc.)

$[Gd(\mathbf{C_{NH2}})_3]^{3+}$ + $2NO_3^-$
Yield: 93%
ESI-MS: $[C_{45}H_{72}GdN_{14}O_{12}]^+$, *m/z*: 1158.4664 (exp.), 1158.4690 (calc.)

$[Gd(\mathbf{E_{N3}})_3]^{3+}$ + $2NO_3^-$
Yield: 97%
ESI-MS: $[C_{33}H_{36}GdN_{14}O_{18}]^+$, *m/z*: 1074.1622 (exp.), 1074.1568 (calc.)

$[Gd(\mathbf{E_{NH2}})_3]^{3+}$ + $2NO_3^-$
Yield: 95%
ESI-MS: $[C_{33}H_{42}GdN_8O_{18}]^+$, *m/z*: 996.1793 (exp.), 996.1853 (calc.)

$[Eu(\mathbf{C_{N3}})_3]^{3+}$ + $2NO_3^-$
Yield: 96%
ESI-MS: $[C_{45}H_{66}EuN_{20}O_{12}]^+$, *m/z*: 1231.4286 (exp.), 1231.4376 (calc.)

$[Eu(\mathbf{C_{NH2}})_3]^{3+}$ + $2NO_3^-$
Yield: 97%
ESI-MS: $[C_{45}H_{72}EuN_{14}O_{12}]^+$, *m/z*: 1153.4667 (exp.), 1153.4661 (calc.)

$[Eu(\mathbf{E_{N3}})_3]^{3+}$ + $2NO_3^-$
Yield: 92%
ESI-MS: $[C_{33}H_{36}EuN_{14}O_{18}]^+$, *m/z*: 1069.1653 (exp.), 1069.1539 (calc.)

$[Eu(\mathbf{E_{NH2}})_3]^{3+}$ + $2NO_3^-$
Yield: 94%
ESI-MS: $[C_{33}H_{42}EuN_8O_{18}]^+$, *m/z*: 991.1901 (exp.), 991.1824 (calc.)

$[Tb(\mathbf{C_{N3}})_3]^{3+}$ + $2NO_3^-$
Yield: 94%
ESI-MS: $[C_{45}H_{66}TbN_{20}O_{12}]^+$, *m/z*: 1237.4410 (exp.), 1237.4417 (calc.)

$[Tb(\mathbf{C_{NH2}})_3]^{3+}$ + $2NO_3^-$
Yield: 92%
ESI-MS: $[C_{45}H_{72}TbN_{14}O_{12}]^+$, *m/z*: 1159.4601 (exp.), 1159.4702 (calc.)

$[Tb(\mathbf{E_{N3}})_3]^{3+}$ + $2NO_3^-$
Yield: 93%
ESI-MS: $[C_{33}H_{36}TbN_{14}O_{18}]^+$, *m/z*: 1075.1852 (exp.), 1075.1580 (calc.)

$[Tb(\mathbf{E_{NH2}})_3]^{3+}$ + $2NO_3^-$
Yield: 93%
ESI-MS: $[C_{33}H_{42}TbN_8O_{18}]^+$, *m/z*: 997.8123 (exp.), 997.8165 (calc.)

3. Results and discussion

3.1. Synthesis and characterization

C_{N3}, **C_{NH2}**, **E_{N3}**, and **E_{NH2}** were synthesized following a modified previously published procedure[15] in 64%, 73%, 32%, and 72% yield, respectively (Scheme 1). The compounds were characterized using NMR and FT-IR spectroscopy, mass spectrometry, and X-ray crystallography (Figs. 3, 4, S1–S16).

C_{N3} crystallized in the monoclinic $P2_1/c$ space group (Table 1, Fig. 3a). Its structure consists of a planar pyridine ring with two carboxamide functional groups at both ortho positions, and an azide functional group at the para position. The dihedral angle of the azide to the pyridyl ring (C2-C3-N4-N5) is 6.40°. Dihedral angles of each carboxamide (N1-C1-C11-N3 and N1-C5-C6-N2) are 68.64° and 82.83°, respectively. The distance between the terminal CH_3 groups, C8 to C13,

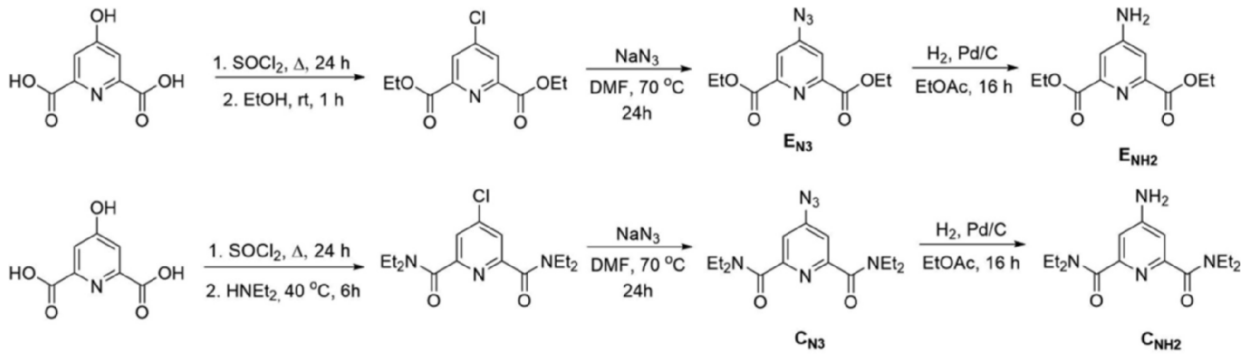

Scheme 1. Synthesis of $\mathbf{C_{N3}}$, $\mathbf{E_{N3}}$, $\mathbf{C_{NH2}}$, and $\mathbf{E_{NH2}}$.

is 5.77 Å. Intermolecular hydrogen bonding [44] interactions were observed, and are shown a dashed lines in Fig. S13, and are comparable to other dipicolinate-based compounds [8,9,45].

$\mathbf{E_{N3}}$ crystallized in the monoclinic $P2_1/c$ space group (Table 1, Fig. 3b). Its structure consists of a planar pyridine ring with diethyl ester functional groups in the ortho positions and an azide functional group at the para position. The dihedral angle of the azide to the pyridyl ring (C4-C3-N2-N3) is 4.37°. Dihedral angles of the N1-C1-C9-O4 and N1-C5-C6-O2 are 7.96° and 5.13°. The distance between the terminal CH_3 groups, C8 to C11, is 6.39 Å. Intermolecular hydrogen bonding [44] interactions are observed and are shown as dashed lines in Fig. S14, and are comparable to other dipicolinate-based compounds. [8,9,45]

$\mathbf{C_{NH2}}$ crystallized in the monoclinic Cc space group (Table 1, Fig. 4a). Its structure consists of a planar pyridine ring with carboxamide functional groups at both ortho positions, and a primary amine at the para position. The dihedral angles of the carbonyl functional groups to the pyridine-N are ~ 117° (N1-C1-C11-N4 and N1-C5-C6-N3). Intermolecular hydrogen bonding[44] interactions are observed and are shown as dashed green lines in Fig. S15, and are comparable to other dipicolinate-based compounds [8,9,45].

$\mathbf{E_{NH2}}$ crystallized in the triclinic P-1 space group (Table 1, Fig. 4b). Its structure consists of a planar pyridine ring with diethyl ester functional groups at both ortho positions, and a primary amine at the para position. The carbonyl groups are nearly planar with the pyridine ring with dihedral angles of N1-C1-C9-O3 = 1.98° and N1-C5-C6-O1 = 0.42°. Intermolecular hydrogen bonding interactions[44] are observed and are shown as dashed green lines in Fig. S16, and are comparable to other dipicolinate-based compounds [8,9,45].

3.2. Emission titrations of C_{N3}, E_{N3}, C_{NH2}, and E_{NH2} with Tb^{III} (speciation)

The stoichiometry of each complex in acetonitrile was determined through emission titration of the ligand with the Tb^{III} nitrate salt (Figs. S20–S23). The emission intensity is highest for 0.33 Tb^{III}:ligand, which is consistent with a 1:3 metal:ligand stoichiometry, as seen for complexes with other dipicolinate derivatives.[9,16,29] Therefore, for spectroscopic characterization, Ln^{III} complexes were synthesized by reacting 3 equivalents of either ligand ($\mathbf{C_{N3}}$, $\mathbf{C_{NH2}}$, $\mathbf{E_{N3}}$, or $\mathbf{E_{NH2}}$) with 1 equivalent of the respective $Ln(NO_3)_3$ salt (Ln^{III} = Eu^{III}, Tb^{III}, or Gd^{III}) in acetonitrile. The speciation for the Eu^{III} complexes, while not done here, should provide similar results, indicating that the 1:3 metal:ligand stoichiometry is stable in solution. The emission lifetimes (*vide infra*) which can be fit to a monoexponential, agree with the presence of a single species in solution for both Eu^{III} and Tb^{III} complexes.

3.3. Singlet and triplet excited state determination

The fluorescence and phosphorescence spectra of $[Gd(\mathbf{L})_3]^{3+}$ ($\mathbf{L}$ = $\mathbf{C_{N3}}$, $\mathbf{C_{NH2}}$, $\mathbf{E_{N3}}$, or $\mathbf{E_{NH2}}$) (Figs. S37–S40) were used to experimentally determine the ligands' ^{1}S and ^{3}T excited states,[40] which are involved in sensitizing Ln^{III} luminescence. ^{1}S and ^{3}T are very similar at ~ 27,100 cm^{-1} and ~ 21,200 cm^{-1}, respectively (Table 2).

The ^{1}S and ^{3}T states have the appropriate energy to sensitize the

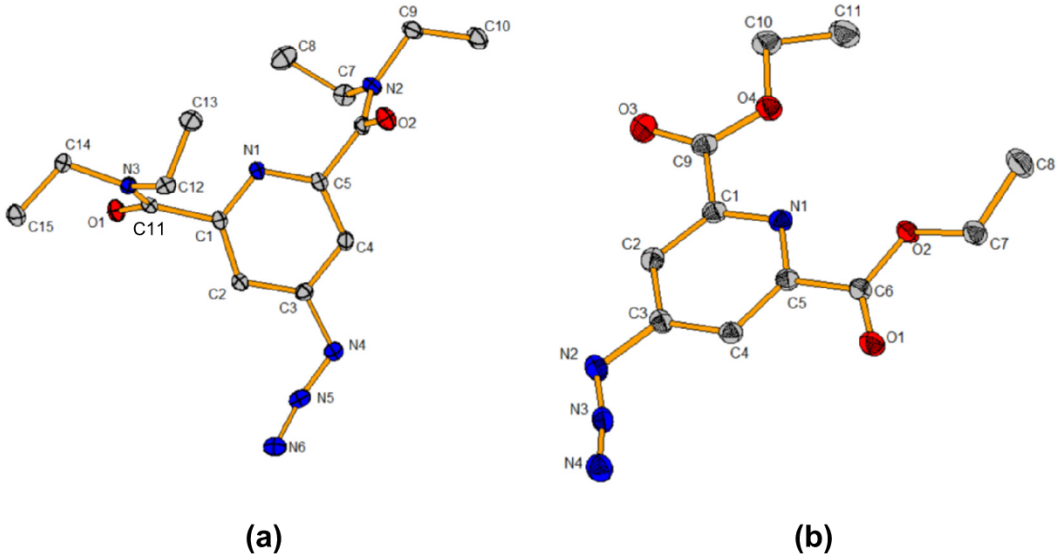

Fig. 3. Thermal ellipsoid plots of (a) $\mathbf{C_{N3}}$ and (b) $\mathbf{E_{N3}}$. Ellipsoids are shown at the 50% probability level. Hydrogen atoms are omitted for clarity.

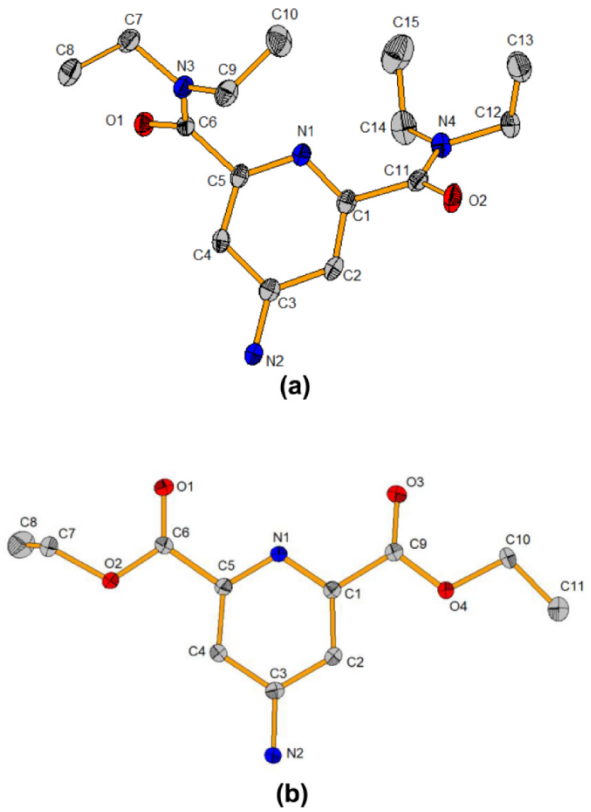

Fig. 4. Thermal ellipsoid plots of (a) $\mathbf{C_{NH2}}$ (b) $\mathbf{E_{NH2}}$. Ellipsoids are shown at the 50% probability level. Hydrogen atoms are omitted for clarity.

emission of both Eu^{III} ($^5D_0$ ~ 17,300 cm^{-1}) and Tb^{III} ($^5D_4$ ~ 20,400 cm^{-1}) and were therefore used to explore the luminescence properties of the respective complexes.[13]

3.4. Absorption and emission properties

$\mathbf{C_{N3}}$, $\mathbf{C_{NH2}}$, $\mathbf{E_{N3}}$, and $\mathbf{E_{NH2}}$ display broad absorption spectra in the UV region (Figs. S17–S19) in acetonitrile with maxima in the range between 250 and 258 nm. This is similar to what was observed for 4-aminopyridine-2,6-dicarboxylic acid,[29] among other *para*-substituted dipicolinate derivatives.[46] When excited at 290 nm, these compounds fluoresce with maxima at 380 nm for the amino derivatives (Figs. S42 & S43), 375 nm for $\mathbf{C_{N3}}$ (Fig. 5), and 378 nm for $\mathbf{E_{N3}}$ (Fig. S41). The excitation spectra of $\mathbf{C_{N3}}$, $\mathbf{C_{NH2}}$, $\mathbf{E_{N3}}$, and $\mathbf{E_{NH2}}$ are all red-shifted from the absorbance maxima. While absorption spectra are indicative of all wavelengths at which the compounds absorb, excitation spectra reflect which of those wavelengths more efficiently lead to

Table 2
^1S and ^3T energies of $[Gd(L)_3]^{3+}$ (L = $\mathbf{C_{N3}}$, $\mathbf{C_{NH2}}$, $\mathbf{E_{N3}}$, or $\mathbf{E_{NH2}}$) in acetonitrile at 77 K.

	^1S (cm^{-1})	^3T (cm^{-1})
$[Gd(\mathbf{C_{N3}})_3]^{3+}$	26,900 ± 150	21,000 ± 200
$[Gd(\mathbf{E_{N3}})_3]^{3+}$	27,000 ± 350	21,200 ± 300
$[Gd(\mathbf{C_{NH2}})_3]^{3+}$	27,400 ± 250	21,200 ± 50
$[Gd(\mathbf{E_{NH2}})_3]^{3+}$	27,200 ± 500	21,500 ± 200

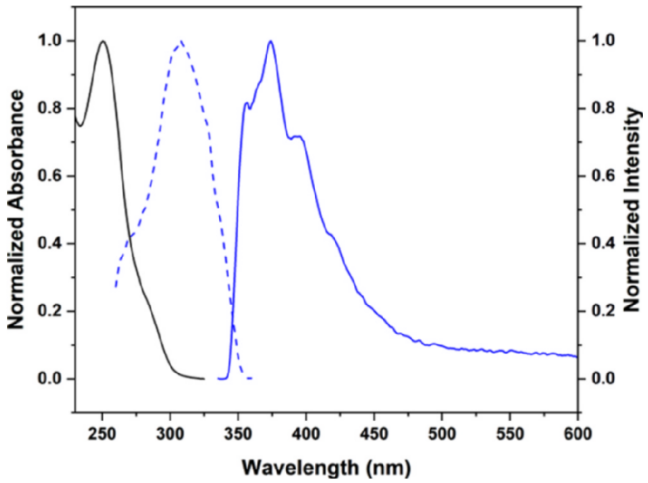

Fig. 5. Normalized absorbance (black), excitation (dashed blue) and emission (solid blue) of $\mathbf{C_{N3}}$ in acetonitrile at 25.0 ± 0.1 °C. λ_{exc} = 290 nm, λ_{em} = 380 nm, [compound] = 1 × 10^{-4} M; slit widths exc = 3.00 nm, em = 1.00 nm. (For interpretation of the references to color in this figure legend, the reader is referred to the web version of this article.)

Table 1
Crystallographic information for $\mathbf{C_{N3}}$, $\mathbf{C_{NH2}}$, $\mathbf{E_{N3}}$, and $\mathbf{E_{NH2}}$.

Compound	$\mathbf{C_{N3}}$	$\mathbf{C_{NH2}}$	$\mathbf{E_{N3}}$	$\mathbf{E_{NH2}}$
CCDC number	1995777	1995780	1995778	1995779
Formula	$C_{15}H_{22}N_6O_2$	$C_{15}H_{24}N_4O_2$	$C_{11}H_{12}N_4O_4$	$C_{11}H_{14}N_2O_4$
M (g/mol)	318.38	292.38	264.25	238.24
Crystal system	monoclinic	monoclinic	monoclinic	triclinic
Space group	$P2_1/c$	Cc	$P2_1/c$	P-1
a (Å)	14.4358(2)	16.0906(2)	15.2768(7)	7.2248(5)
b (Å)	8.9532(1)	10.9478(2)	4.3205(2)	9.1046(7)
c (Å)	13.1406(2)	12.2404(2)	19.2297(8)	9.1973(6)
α(°)	90	90	90	69.891(5)
β	103.6205(5)	130.474(4)	106.529(3)	79.525(4)
γ(°)	90	90	90	89.877(5)
V ($Å^3$)	1650.61(4)	1640.23(6)	1216.78(10)	557.45(7)
T (K)	100(2)	100(2)	100(2)	100(2)
Z	4	4	4	2
D_c (g/cm^3)	1.281	1.184	1.442	1.419
μ (Mo-Kα) (1/mm)	0.089	0.081	0.113	0.109
Independent reflections, R_{int} [$F_o \geq 4\sigma(F_o)$]	5053, 0.0285	3258, 0.0330	3003, 0.0355	2280, 0.0275
Reflections collected	42,169	11,742	14,811	5180
Data/restraints/parameters	5053 / 0 / 212	3258 / 2 / 194	3003 / 0 / 174	2280 / 0 / 156
Goodness-of-fit on F^2	1.029	1.041	1.056	1.070
R_1, wR_2 (all data)	0.0362, 0.09570.0436, 0.1023	0.0375, 0.07770.0508, 0.0842	0.0363, 0.09720.0416, 0.1024	0.0629, 0.17400.0679, 0.1788
Largest diff. peak and hole/ ($e/Å^3$)	0.735 and −0.198	0.167 and −0.162	0.468 and −0.244	0.900 and −0.636

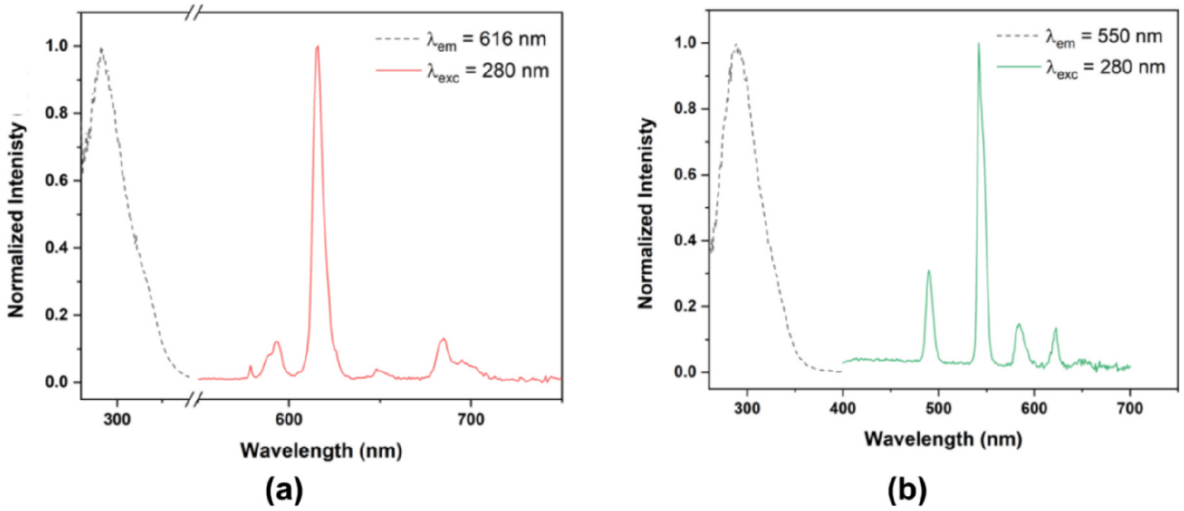

Fig. 6. (a) Normalized excitation (dashed) and emission spectra (solid) of $[Eu(\mathbf{E_{N3}})_3]^{3+}$; (b) normalized excitation (dashed) and emission spectra (solid) of $[Tb(\mathbf{E_{N3}})_3]^{3+}$. All spectra were measured in acetonitrile at 25.0 ± 0.1 °C (λ_{exc} = 280 nm). [complex] = 5 × 10^{-5} M; slit widths exc = 3.00 nm, em = 1.00 nm.

emission and thus the bathochromic shift.

When excited at 280 nm, $[Eu(\mathbf{L})_3]^{3+}$ and $[Tb(\mathbf{L})_3]^{3+}$ (**L** = $\mathbf{C_{N3}}$, $\mathbf{C_{NH2}}$, $\mathbf{E_{N3}}$, or $\mathbf{E_{NH2}}$) luminesce in the visible region, and the characteristic metal-centered emission peaks were observed (Eu^{III}: $^5D_0 \rightarrow {}^7F_J$ (J = 0 – 4); Tb^{III}: $^5D_4 \rightarrow {}^7F_J$ (J = 6 – 2); Fig. 6, and S41 – S43). For Eu^{III}, in all cases, the $^5D_0 \rightarrow {}^7F_2$ transition appears as a single peak. Yet, despite the lack of fine structure, the presence of the $^5D_0 \rightarrow {}^7F_0$ transition is consistent with a pseudo-D_3 symmetry around the metal ion, as seen for other dipicolinato-based complexes with a 1:3 stoichiometry. [15,29,46]

The quantum yields of sensitized emission (ϕ_{Eu} and ϕ_{Tb}) for all complexes were determined in acetonitrile and are summarized in Table 3. For emission for $[Eu(\mathbf{C_{N3}})_3]^{3+}$ ϕ_{Eu} is 0.11%, for $[Eu(\mathbf{E_{N3}})_3]^{3+}$ is 0.15%, for $[Eu(\mathbf{C_{NH2}})_3]^{3+}$ is 13.8%, and for $[Eu(\mathbf{E_{NH2}})_3]^{3+}$ is 14.4%. The amino-derivatives are moderately efficient sensitizers of Eu^{III}, and compare favorably to other dipicolinate derivatives.[15,21,29,47] Surprisingly, the azido-derivatives are not very efficient sensitizers, despite their similar structure and excited energy levels, with efficiencies that are orders of magnitude lower than the amino-derivatives (*vide infra*).

For emission for $[Tb(\mathbf{C_{N3}})_3]^{3+}$ ϕ_{Tb} is 0.30%, for $[Tb(\mathbf{E_{N3}})_3]^{3+}$ is 0.27%, for $[Tb(\mathbf{C_{NH2}})_3]^{3+}$ is 29.7%, and for $[Tb(\mathbf{E_{NH2}})_3]^{3+}$ is 28.9% (Table 3). The Tb^{III} complexes show a similar trend in emission efficiency as seen for the Eu^{III} complexes; the amino-derivatives are moderately efficient at sensitizing Tb^{III}, yet the azido-derivatives are significantly less efficient. The efficiencies of the former complexes are similar to other Tb^{III} complexes based on the dipicolinate scaffold. [21,29]

The emission decay lifetimes for the Eu^{III} compounds (τ_{Eu}) are 0.54 ms, 0.65 ms, 1.18 ms, and 1.37 ms, respectively (Table 3). The emission decay lifetimes for the Tb^{III} compounds (τ_{Tb}) are 0.21 ms, 0.25 ms, 0.88 ms, and 0.63 ms, respectively (Table 3). The decay curves for all Ln^{III} complexes could fit a single exponential decay (Table S1, Figs. S44–S51), indicating that there is one coordination environment around each metal ion. These lifetimes are comparable to other similar dipicolinate-based luminescent Eu^{III} and Tb^{III} complexes.[18,19,29,48]

The τ_{Ln} are shorter, and the ϕ_{Ln} are decreased for the azido-derivatives when compared to the amino-derivatives, yet their ^3T states are similar in energy. This suggests that inefficient energy transfer from the ^3T state of azido-derivatives to the Ln^{III} metal is not the cause of this discrepancy, which is further confirmed by the absence of ligand emission within the luminescence spectrum.

Werts and co-workers[42] demonstrated that we could easily determine ϕ_{Ln}^{Ln} and η_{sens} for Eu^{III}, and thus, we can use the metal complexes of this ion to further analyze the emission process. As seen in Table 3, η_{sens} is 0.6% for the azido- derivatives and 29% for the amino-derivatives, which confirms that the amino- derivatives are better sensitizers of Eu^{III} emission that the azido-derivatives. The values of ϕ_{Eu}^{Eu} are higher for the amino-derivatives as well, indicating that these ligands might prevent vibrational quenching of Eu^{III} luminescence more effectively than the azido-derivatives. Nonetheless, the overall lower values for ϕ_{Ln}, ϕ_{Eu}^{Eu}, and η_{sens} for the azido-derivatives are more likely related to a lack of stability of the organic azido-derivatives,[49] which we observed as color changes of the solutions from colorless to dark after UV light irradiation for longer than 5 s, and reflected in a decrease in emission intensity of the organic compounds, $\mathbf{C_{N3}}$ and $\mathbf{E_{N3}}$, on their own over time. This instability results in a decrease in emission intensity of the complexes as well, as shown in Fig. S52, although emission lifetimes and spectral shape are retained. Attempts to identify the product of this decomposition using FT-IR spectroscopy, NMR spectroscopy, and mass spectrometry are ongoing.

3.5. Conclusions

New dipicolinato-based compounds were synthesized and characterized to assess their ability to sensitize visible emitting Ln^{III} (Eu^{III}, Tb^{III}). The ligands' ^1S and ^3T excited states were determined for all ligands and are approximately ~ 27,100 cm^{-1} and ~ 21,200 cm^{-1},

Table 3
Quantum yields of sensitized emission (ϕ_{Ln}), luminescence lifetimes (τ_{Ln}), intrinsic quantum yield for Eu^{III} complexes (ϕ_{Eu}^{Eu}), and sensitization efficiency (η_{sens}) for $[Ln(\mathbf{L})_3]^{3+}$ in acetonitrile at 25.0 ± 0.1 °C (Ln^{III} = Eu^{III}, Tb^{III}).

		ϕ_{Eu} (%)	τ_{Eu} (ms)	ϕ_{Eu}^{Eu} (%)	η_{sens} (%)	ϕ_{Tb} (%)	τ_{Tb} (ms)
azido	$[Ln(\mathbf{C_{N3}})_3]^{3+}$	0.11 ± 0.01	0.54 ± 0.01	19	0.6	0.30 ± 0.03	0.21 ± 0.06
	$[Ln(\mathbf{E_{N3}})_3]^{3+}$	0.15 ± 0.01	0.65 ± 0.04	24	0.6	0.27 ± 0.02	0.25 ± 0.01
amino	$[Ln(\mathbf{C_{NH2}})_3]^{3+}$	13.8 ± 0.7	1.18 ± 0.00	47	29	29.7 ± 0.9	0.88 ± 0.02
	$[Ln(\mathbf{E_{NH2}})_3]^{3+}$	14.4 ± 0.2	1.37 ± 0.00	50	29	28.9 ± 0.3	0.63 ± 0.01

respectively. The amino-containing ligands are more efficient at sensitizing Eu^{III} and Tb^{III}, with the highest efficiencies at ϕ_{Tb} = 29.7% for $[Tb(\mathbf{C_{NH2}})_3]^{3+}$ and ϕ_{Eu} = 14.4% for $[Eu(\mathbf{E_{NH2}})_3]^{3+}$ when compared to the azido-based compounds, which have efficiencies of 0.11% and 0.14% for $[Eu(\mathbf{C_{N3}})_3]^{3+}$ and $[Eu(\mathbf{E_{N3}})_3]^{3+}$, and 0.30% and 0.27% for $[Tb(\mathbf{C_{N3}})_3]^{3+}$ and $[Tb(\mathbf{E_{N3}})_3]^{3+}$, respectively. Because there are no significant differences in ^{3}T state to help rationalize the observed photophysical behavior, further investigation indicated that the azido-derivatives are light-sensitive, resulting in decomposition products that do not sensitize Ln^{III} efficiently. The good emission efficiencies observed for the complexes with the amino ligands make them promising for applications such as bioimaging, lighting, and sensing.

CRediT authorship contribution statement

Katherine R. Johnson: Data curation, Formal analysis, Writing of manuscript first draft. **Ana de Bettencourt-Dias:** Conceptualization, Funding acquisition, Project administration, Resources, Supervision, Writing - review & editing.

Declaration of Competing Interest

The authors declare that they have no known competing financial interests or personal relationships that could have appeared to influence the work reported in this paper.

Acknowledgments

Financial support of this work through the National Science Foundation is gratefully acknowledged (Grant CHE 1800392). Janina S. Ruprecht is acknowledged for her support with mass spectrometry. Dominion R. Fredericks is acknowledged for his support with ^{13}C-NMR and FT-IR data collection.

Appendix A. Supplementary data

Supplementary data to this article can be found online at https://doi.org/10.1016/j.ica.2020.120003.

References

[1] D. Parker, J. Yu, A pH-insensitive, ratiometric chemosensor for citrate using europium luminescence, Chem. Commun. (2005) 3141–3143.
[2] A. Jana, B.J. Crowston, J.R. Shewring, L.K. McKenzie, H.E. Bryant, S.W. Botchway, A.D. Ward, A.J. Amoroso, E. Baggaley, M.D. Ward, Heteronuclear Ir(III)-Ln(III) Luminescent Complexes: Small-Molecule Probes for Dual Modal Imaging and Oxygen Sensing, Inorg. Chem. 55 (2016) 5623–5633.
[3] W. Liu, C. Chen, X. Huang, E. Xie, W. Liu, Functional construction of dual-emitting 4-aminonaphthalimide encapsulated lanthanide MOFs composite for ratiometric temperature sensing, Chem.: Eur. J 25 (2019) 10054.
[4] M. Liu, Z. Ye, C. Xin, J. Yuan, Development of a ratiometric time-resolved luminescence sensor for pH based on lanthanide complexes, Anal. Chim. Acta 761 (2013) 149–156.
[5] A. Maroń, S. Kula, A. Szlapa-Kula, A. Świtlicka, B. Machura, S. Krompiec, J.G. Małecki, R. Kruszyński, A. Chrobok, E. Schab-Balcerzak, S. Kotowicz, M. Siwy, K. Smolarek, S. Maćkowski, H. Janeczek, M. Libera, 2,2′:6′,2″-Terpyridine Analogues: Structural, Electrochemical, and Photophysical Properties of 2,6-Di(thiazol-2-yl)pyridine Derivatives, Eur. J. Org. Chem. 19 (2017) 2730–2745.
[6] A.Y. Ku, A.A. Setlur, J. Loudis, Impact of light emitting diode adoption on rare earth element use in lighting: Implications for yttrium, europium, and terbium demand, Electrochem. Soc. Interface 24 (2015) 45–49.
[7] M.H.V. Werts, R.H. Woudenberg, P.G. Emmerink, R. van Gassel, J.W. Hofstraat, J.W. Verhoeven, A Near-Infrared Luminescent Label Based on Yb^{III} Ions and Its Application in a Fluoroimmunoassay, Angew. Chem. 39 (2000) 4542–4544.
[8] A. de Bettencourt-Dias, S. Viswanathan, A. Rollett, Thiophene-Derivatized Pybox and Its Highly Luminescent Lanthanide Ion Complexes, J. Am. Chem. Soc. 129 (2007) 15436–15437.
[9] A. de Bettencourt-Dias, P.S. Barber, S. Bauer, A Water-Soluble Pybox Derivative and Its Highly Luminescent Lanthanide Ion Complexes, J. Am. Chem. Soc. 134 (2012) 6987–6994.
[10] U. Cho, D.P. Riordan, P. Ciepla, K.S. Kocherlakota, J.K. Chen, P.B. Harbury, Ultrasensitive optical imaging with lanthanide lumiphores, Nat. Chem. Biol. 14 (2017) 15–21.
[11] B. Brennecke, Q. Wang, Q. Zhang, H.-Y. Hu, M. Nazaré, An Activatable Lanthanide Luminescent Probe for Time-Gated Detection of Nitroreductase in Live Bacteria, Angewan. Chem. Int. Ed. 59 (2020) 8512–8516.
[12] N. Hamon, A. Roux, M. Beyler, J.-C. Mulatier, C. Andraud, C. Nguyen, M. Maynadier, N. Bettache, A. Duperray, A. Grichine, S. Brasselet, M. Gary-Bobo, O. Maury, R. Tripier, Pyclen-Based Ln(III) Complexes as Highly Luminescent Bioprobes for In Vitro and In Vivo One- and Two-Photon Bioimaging Applications, J. Am. Chem. Soc. 142 (2020) 10184–10197.
[13] M. Latva, H. Takalo, V.-M. Mukkala, C. Matachescu, J.C. Rodríguez-Ubis, J. Kankare, Correlation between the lowest triplet state energy level of the ligand and lanthanide(III) luminescence quantum yield, J. Lumin. 75 (1997) 149–169.
[14] K.R. Johnson, S.B. Vittardi, M.A. Gracia-Nava, J.J. Rack, A. de Bettencourt-Dias, Wavelength-dependent singlet oxygen generation in luminescent lanthanide complexes with a pyridine-bis(carboxamide)-terthiophene sensitizer, Chem. Eur. J. (2020), https://doi.org/10.1002/chem.202000587.
[15] K.R. Johnson, A. de Bettencourt-Dias, $^1O_2$ generating luminescent lanthanide complexes with 1,8-naphthalimide-based sensitizers, Inorg. Chem. 58 (2019) 13471–13480.
[16] J.H.S.K. Monteiro, F.A. Sigoli, A. de Bettencourt-Dias, A water-soluble Tb^{III} complex as a temperature-sensitive luminescent probe, Can. J. Chem. 96 (2017) 859–864.
[17] P.A. Brayshaw, J.-C.-G. Buenzli, P. Froidevaux, J.M. Harrowfield, Y. Kim, A.N. Sobolev, Synthetic, Structural, and Spectroscopic Studies on Solids Containing Tris(dipicolinato) Rare Earth Anions and Transition or Main Group Metal Cations, Inorgan. Chem. 34 (1995) 2068–2076.
[18] A.S. Chauvin, F. Gumy, D. Imbert, J.C.G. Bünzli, Europium and Terbium tris (Dipicolinates) as Secondary Standards for Quantum Yield Determination, Spectrosc. Lett. 37 (2004) 517–532.
[19] A.-S. Chauvin, F. Gumy, D. Imbert, J.-C.G. Bunzli, Erratum to "Europium and Terbiumtris(Dipicolinates) as Secondary Standards for Quantum Yield Determination", Spectrosc. Lett., 40 (2007) 193-193.
[20] A. Picot, C. Feuvrie, C. Barsu, F. Malvolti, B. Le Guennic, H. Le Bozec, C. Andraud, L. Toupet, O. Maury, Synthesis, structures, optical properties, and TD-DFT studies of donor-π-conjugated dipicolinic acid/ester/amide ligands, Tetrahedron 64 (2008) 399–411.
[21] A.-L. Gassner, C. Duhot, J.-C.-G. Bünzli, A.-S. Chauvin, Remarkable Tuning of the Photophysical Properties of Bifunctional Lanthanide tris(Dipicolinates) and its Consequence on the Design of Bioprobes, Inorg. Chem. 47 (2008) 7802–7812.
[22] A. Aebischer, F. Gumy, J.-C.-G. Bünzli, Intrinsic quantum yields and radiative lifetimes of lanthanide tris(dipicolinates), Phys. Chem. Chem. Phys. 11 (2009) 1346–1353.
[23] S.V. Eliseeva, G. Auböck, F. van Mourik, A. Cannizzo, B. Song, E. Deiters, A.-S. Chauvin, M. Chergui, J.-C.-G. Bünzli, Multiphoton-Excited Luminescent Lanthanide Bioprobes: Two- and Three-Photon Cross Sections of Dipicolinate Derivatives and Binuclear Helicates, J. Phys. Chem. B 114 (2010) 2932–2937.
[24] C.R. Heathman, K.L. Nash, Characterization of Europium and Americium Dipicolinate Complexes, Separat. Sci. Technol. 47 (2012) 2029–2037.
[25] J. Andres, R.D. Hersch, J.-E. Moser, A.-S. Chauvin, A New Anti-Counterfeiting Feature Relying on Invisible Luminescent Full Color Images Printed with Lanthanide-Based Inks, Adv. Funct. Mater. 24 (2014) 5029–5036.
[26] J. Andres, K.E. Borbas, Expanding the Versatility of Dipicolinate-Based Luminescent Lanthanide Complexes: A Fast Method for Antenna Testing, Inorg. Chem. 54 (2015) 8174–8176.
[27] M.A. Melo Lucena, M.O. Rodrigues, C.C. Gatto, M. Talhavini, A.O. Maldaner, S. Alves, I.T. Weber, Synthesis of [Dy(DPA)(HDPA)] and its potential as gunshot residue marker, J. Lumin. 170 (2016) 697–700.
[28] J.H.S.K. Monteiro, N.R. Fetto, M.J. Tucker, A. de Bettencourt-Dias, Luminescent carbazole-based Eu^{III} and Yb^{III} complexes with a high two-photon absorption cross-section enable viscosity sensing in the visible and near IR with one- and two-photon excitation, Inorg. Chem. 59 (2020) 3193–3199.
[29] J.H.S.K. Monteiro, D. Machado, L.M. de Hollanda, M. Lancellotti, F.A. Sigoli, A. de Bettencourt-Dias, Selective cytotoxicity and luminescence imaging of cancer cells with a dipicolinato-based Eu^{III} complex, Chem. Commun. 53 (2017) 11818–11821.
[30] M. Stocks, The small molecule drug discovery process – from target selection to candidate selection, in: R. Ganellin, S. Roberts, R. Jefferis (Eds.), Introduction to Biological and Small Molecule Drug Research and Development, Elsevier, Oxford, 2013, pp. 81–126.
[31] H.C. Kolb, K.B. Finn, B. Sharpless, Click Chemistry: Diverse Chemical Function from a Few Good Reactions, Angew. Chem. Int. Ed. 40 (2001) 2004–2021.
[32] J.-C.-G. Bünzli, Lanthanide luminescence for biomedical analyses and imaging, Chem. Rev. 110 (2010) 2729–2755.
[33] Z. Tang, Z. Lin, G. Li, Y. Hu, Amino Nitrogen Quantum Dots-Based Nanoprobe for Fluorescence Detection and Imaging of Cysteine in Biological Samples, Anal. Chem. 89 (2017) 4238–4245.
[34] Q. Ju, D. Tu, Y. Liu, R. Li, H. Zhu, J. Chen, Z. Chen, M. Huang, X. Chen, Amine-functionalized lanthanide-doped $KGdF_4$ nanocrystals as potential optical/magnetic multimodal bioprobes, J. Am. Chem. Soc. 134 (2012) 1323–1330.
[35] G.J. Stasiuk, N.J. Long, The ubiquitous DOTA and its derivatives: the impact of 1,4,7,10-tetraazacyclododecane-1,4,7,10-tetraacetic acid on biomedical imaging, Chem. Commun. 49 (2013) 2732–2746.
[36] R.D. Teo, J. Termini, H.B. Gray, Lanthanides: Applications in Cancer Diagnosis and Therapy, J. Med. Chem. 59 (2016) 6012–6024.
[37] S. Dasari, S. Singh, S. Sivakumar, A.K. Patra, Dual-Sensitized Luminescent Europium(III) and Terbium(III) Complexes as Bioimaging and Light-Responsive Therapeutic Agents, Chemistry – A, European Journal 22 (2016) 17387–17396.
[38] SADABS: v. 2.01 An empirical absorption correction program., in, Bruker AXS Inc., Madison, WI., 2001.

[39] SHELXTL: v.6.10 Structure Determination Software Suite., in: Sheldrick GM (Ed.), Bruker AXS Inc., Madison, WI., 2001.
[40] G.A. Crosby, R.E. Whan, R.M. Alire, Intramolecular Energy Transfer in Rare Earth Chelates. Role of the Triplet State, J. Chem. Phys. 34 (1961) 743–748.
[41] P.H. Hänninen, H., Lanthanide Luminescence Photophysical, Analytical and Biological Aspects, 1 ed., Springer-Verlag Berlin Heidelberg, 2011.
[42] M.H.V. Werts, R.T.F. Jukes, J.W. Verhoeven, The emission spectrum and the radiative lifetime of Eu^{3+} in luminescent lanthanide complexes, Phys. Chem. Chem. Phys. 4 (2002) 1542–1548.
[43] G.F. de Sá, O.L. Malta, C. de Mello Donegá, A.M. Simas, R.L. Longo, P.A. Santa-Cruz, E.F. da Silva, Spectroscopic properties and design of highly luminescent lanthanide coordination complexes, Coord. Chem. Rev. 196 (2000) 165–195.
[44] G.R. Desiraju, T. Steiner, The weak hydrogen bond: in structural chemistry and biology, International Union of Crystal, 2001.
[45] R.A. Tigaa, A. de Bettencourt-Dias, Synthesis and Characterization of Two Tritylthio-Derivatives: 1-Bromo-3-Tritylthiopropane and 2-(Tritylthio)-Ethanethiol, J. Chem. Crystallogr. 47 (2017) 233–240.
[46] R.A. Tigaa, X. Aerken, A. Fuchs, A. de Bettencourt-Dias, Sensitization of LnIII (Ln = Eu, Tb, Tm) Ion Luminescence by Functionalized Polycarbonate-Based Materials and White Light Generation, Eur. J. Inorg. Chem. (2017) 5310–5317.
[47] K.R. Johnson, M.A. Gracia-Nava, A. de Bettencourt Dias, Thiophene-derivatized pyridine-biscarboxamide as a sensitizer for Ln^{III} luminescence and $^1O_2$ generation, J. Lumin. 49 (2020) 6661–6667.
[48] D. Kovacs, S.R. Kiraev, D. Phipps, A. Orthaber, K.E. Borbas, Eu(III) and Tb(III) Complexes of Octa- and Nonadentate Macrocyclic Ligands Carrying Azide, Alkyne, and Ester Reactive Groups, Inorg. Chem. 59 (2020) 106–117.
[49] G. L'abbe, Decomposition and addition reactions of organic azides, Chem. Rev., 69 (1969) 345-363.